Journal of the Ceramic Society of Japan 126 [7] 568-572 2018
DOI http://doi.org/10.2109/jcersj2.18011

JCS-Japan

FULL PAPER

Synthesis of submicron-sized $NiPS_3$ particles and electrochemical properties as active materials in all-solid-state lithium batteries

Yusaku SUTO[1], Yuta FUJII[1], Akira MIURA[2,†], Nataly Carolina ROSERO-NAVARRO[2], Mikio HIGUCHI[2] and Kiyoharu TADANAGA[2]

[1]Graduate School of Chemical Sciences and Engineering, Hokkaido University, Sapporo 060–8628, Japan
[2]Faculty of Engineering, Hokkaido University, Sapporo 060–8628, Japan

Submicron-sized $NiPS_3$ particles were synthesized by heating fine Ni powder (<100 nm), red phosphorus, and sulfur at 673 K for 48 h, and their electrochemical properties as cathodes in sulfide-based all-solid-state lithium batteries were investigated using discharge/charge measurements, X-ray diffraction (XRD) measurements, electrochemical impedance spectroscopy, and X-ray absorption near-edge structure spectroscopy (XANES). Batteries using submicron-sized $NiPS_3$ as a cathode active material exhibited a 10th discharge capacity of 147 mAh g^{-1}, which was larger than that obtained with 10–100 micron-sized $NiPS_3$ (~90 mAh g^{-1}). The XRD patterns of the composite cathode before and after discharge/charge suggested that $Li_4P_2S_6$ was formed irreversibly ($2NiPS_3 + 4Li^+ + 4e^- \rightarrow Li_4P_2S_6 + 2Ni$), and this irreversible reaction would reduce the capacity of the cathode. The XANES spectra suggested the oxidation/reduction of Ni during discharge–charge cycles, but the change in the spectra during the cycles was considerably small if one assumed the oxidation/reduction of Ni^{2+}/Ni^0.

Key-words : All-solid-state lithium secondary battery, Sulfide

[Received January 17, 2018; Accepted April 17, 2018]

1. Introduction

All-solid-state lithium secondary batteries have attracted much attention as a next generation energy storage device due to their safety, durability, and specific energy.[1),2)] High lithium ion conductive electrodes and low interface resistance between the electrode and solid electrolyte are important factors that can improve the performance of such batteries.[3)–5)] Sulfide solid electrolytes are well known for their high lithium conductivity[6)–13)] and have been used in all-solid-state lithium secondary batteries.[12)–15)] Owing to their deformability, sulfide electrolytes present the advantage of decreasing grain-boundary resistance by a cold- or warm-press process.[16),17)]

To maximize the merits of sulfide electrolytes, a low resistive interface between the electrode and electrolyte is essential for Li^+ diffusion.[18)–20)] However, the formation of low interface resistance between electrode and electrolyte is difficult. For example, the formation of an interfacial layer from the diffusion of component elements of the electrodes or electrolytes is one of the causes of boundary resistance.[21)–24)] Accordingly, our group has focused on $NiPS_3$ electrodes because a favorable interface can be formed between the Li_2S–P_2S_5 glass electrolyte and the $NiPS_3$ electrodes. As Li_2S–P_2S_5 electrolytes are composed of PS_4^{3-}, $P_2S_7^{4-}$, and/or $P_2S_6^{4-}$ units[25)] and $NiPS_3$ also possesses a $P_2S_6^{4-}$ unit,[26)] the diffusion of components is not expected to form a layer with high resistivity.

$NiPS_3$ has a layered structure, and it has been reported that 1.5 mol of Li^+ can be accommodated in the interlayer, which corresponds to a theoretical capacity of 216 mAh g^{-1}, according to the following reaction [Eq. (1)].[27)]

$$NiPS_3 + xLi^+ + xe^- \rightleftarrows Li_xNiPS_3 \ (0 \le x \le 1.5) \quad (1)$$

Studies on the crystal structure and electrochemical properties of $NiPS_3$ and on liquid type lithium batteries employing $NiPS_3$ as cathode have been reported.[28)] Our group has demonstrated the operation of an all-solid-state lithium battery using $NiPS_3$/$FePS_3$ and a sulfide-based solid electrolyte.[29),30)] The all-solid-state cell using 10 to 100-μm sized $NiPS_3$ particles showed a stable capacity of ca. 80 mAh g^{-1} for 30 cycles, indicating that $NiPS_3$ is a promising active material for all-solid-state lithium batteries. However, this discharge capacity was quite smaller than the theoretical capacity; therefore, the performance of the active material can be improved.

Herein, we synthesized submicron-sized $NiPS_3$ particles and applied them as the cathode active material in sulfide-based all-solid-state lithium batteries. In addition, we examined the X-ray diffraction (XRD) and Ni K-edge X-ray absorption near-edge structure spectroscopy (XANES) spectra of the working electrode to reveal the degradation mechanism of the $NiPS_3$ active material.

† Corresponding author: A. Miura; E-mail: amiura@eng.hokudai.ac.jp

2. Experimental procedures

$NiPS_3$ powders were synthesized by heating the following starting materials: Ni powder (<100 nm) (Aldrich, 99%), red phosphorus (Kanto Chemical, 98%), and sulfur (Kanto Chemical, 99.5%). The Ni powder was put in a quartz glass ampoule with 20 mass % excess of phosphorus and sulfur. The mixture in the ampoule was heated at 673 K for 48 h. After heating, the product was washed with water and filtrated to remove the excess P–S compounds. XRD measurements were performed with a diffractometer (Rigaku, MiniFlex600) using Cu Kα radiation. The morphology of the $NiPS_3$ powders was observed with a scanning electron microscope (JEOL, JSM-6390LVS).

All-solid-state cells of Li–In/$80Li_2S{\cdot}20P_2S_5$/$NiPS_3$ were fabricated to investigate the electrochemical properties of $NiPS_3$ as an active material. All the processes were conducted in a dry box filled with dry Ar gas. $80Li_2S{\cdot}20P_2S_5$ was synthesized by mechanical milling. Reagent-grade Li_2S (Mitsuwa Chemical, 99.9%) and P_2S_5 (Aldrich, 99%) were mixed using an agate mortar and pestle, and the mixture was put in a zirconium oxide pot (Fritsch, 45 mL) with zirconium oxide balls (4 mm of diameter). The mixture was mechanically milled using a planetary ball milling apparatus (Ito Seisakusho, LP-M2) for 10 h at 510 rpm.

The Li–In/$80Li_2S{\cdot}20P_2S_5$/$NiPS_3$ cell was fabricated by a uniaxial cold-press method. The $NiPS_3$ composite, which is a mixture of $NiPS_3$, $80Li_2S{\cdot}20P_2S_5$, and Vapor-Grown Carbon Fiber (VGCF: Showa Denko) in the weight ratio of 69:29:2, was used as the cathode of the batteries. $80Li_2S{\cdot}20P_2S_5$ was used as a solid electrolyte, and Li–In was used as the anode. In a polycarbonate tube (10 mm of diameter), 10 mg of $NiPS_3$ composite and 120 mg of solid electrolyte were pelletized by cold-pressing at 360 MPa. Li–In alloy foil was printed on the pellet face at 120 MPa. The prepared pellet was inserted between stainless-steel disks that act as current collectors. The electrochemical properties were evaluated using a charge–discharge measurement device (Scribner Associates Inc., 580 battery test system) and an impedance analyzer (Solartron 1287 coupled with Solartron 1260). Electrochemical measurements were conducted at room temperature. To examine the degradation mechanism of $NiPS_3$ in all-solid-state batteries, all-solid-state cells were prepared using $75Li_2S{\cdot}25P_2S_5$ glass. Glassy $75Li_2S{\cdot}25P_2S_5$ prepared by mechanical milling does not contain crystalline phases and is thus suitable for XRD studies. The XANES spectra at the Ni K-edge of the $NiPS_3$ composite were measured on the BL11S2 beamline at the Aichi Synchrotron Radiation Center (Proposal No. 201605040) to observe the reduction and oxidation of Ni before and after the discharge–charge.

3. Results

Figures 1(a) and 1(b) show the XRD pattern and scanning electron microscope (SEM) image of the prepared $NiPS_3$ powders, respectively. $NiPS_3$ was observed as a single phase. In Fig. 1(b), hexagonal plate of $NiPS_3$ less than 1 µm in size are observed. These particles are much smaller than those synthesized at 998 K for 24 h as reported in our previous paper (10–100 µm).[29]

Figure 2 shows the discharge–charge curves of the Li–In/$80Li_2S{\cdot}20P_2S_5$/$NiPS_3$ all-solid-state cell at 0.064 mA cm^{-2}. The measurement began with a discharge process, i.e., Li^+ insertion into $NiPS_3$. In this initial discharge, the capacity reached 216 mAh g^{-1}, which corresponds to

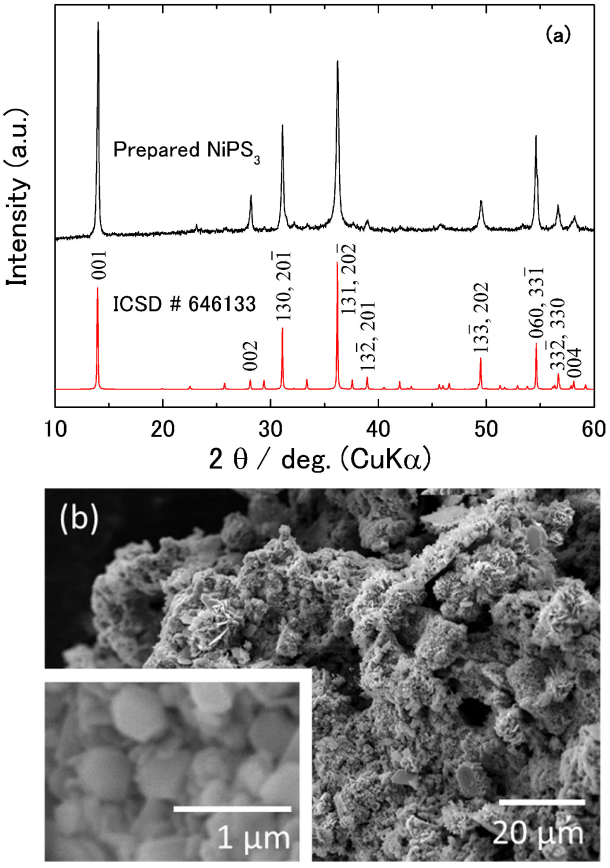

Fig. 1. (a) XRD pattern of the $NiPS_3$ powders. The bottom is the simulated diffraction pattern using ICSD #646133. (b) SEM images of the $NiPS_3$ powders. The inset shows magnified image.

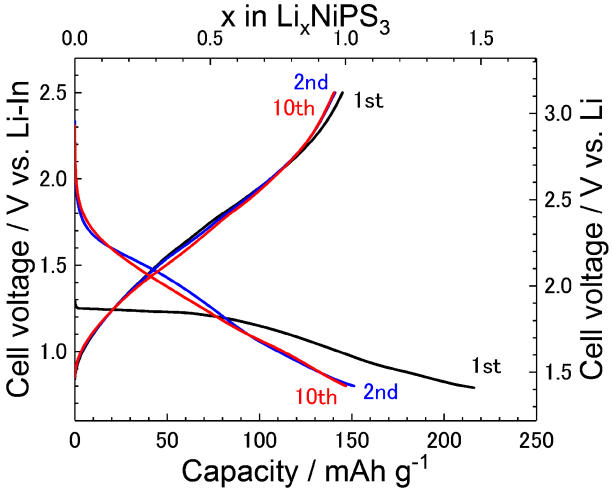

Fig. 2. Discharge–charge curves of the Li–In/$80Li_2S{\cdot}20P_2S_5$/$NiPS_3$ cell cycled between 0.8–2.5 V vs. Li–In.

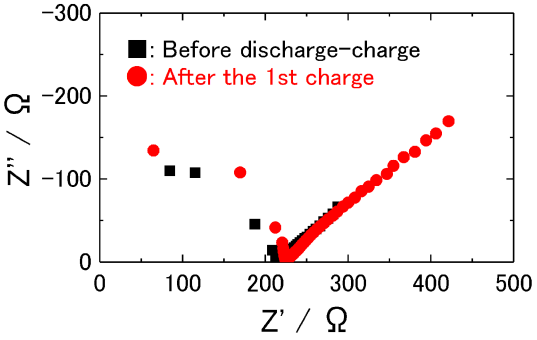

Fig. 3. Impedance profiles of Li–In/80Li_2S·20P_2S_5/$NiPS_3$ cells before and after the 1st discharge–charge.

the theoretical capacity of the insertion reaction [Eq. (1)]. After the initial discharge, the cell was charged and discharged with a cut-off voltage of 0.8–2.5 V. The 10th discharge capacity was 147 mAh g^{-1}. After the 1st cycle, a change in the discharge behavior was observed, which could be explained by the degradation of crystallinity[31] and/or the decomposition of $NiPS_3$ described later. The discharge capacity of the cell in this study was larger than that of the cell using 10–100 µm-sized $NiPS_3$ electrodes.[29]

The impedance profiles before and after the 1st cycle of the Li–In/80Li_2S·20P_2S_5/$NiPS_3$ cell are presented in **Fig. 3**. The semicircles in the high frequency range were ascribed to the solid electrolyte layer of the pellets. There is no obvious difference between the two profiles. Large interfacial resistance was not observed after the 1st charge even though the formation of a highly resistive layer in sulfide-based all-solid-state lithium secondary batteries after cycling has been reported.[21)–24)]

The XRD patterns of the as-prepared $NiPS_3$ and of the working electrodes after the 1st discharge and charge are shown in **Figs. 4**(a)–4(c), respectively. Well-crystallized $NiPS_3$ are visible in Fig. 4(a). However, after the 1st discharge, the intensity of the diffraction peaks of $NiPS_3$ decreased [Fig. 4(b)]. No other diffraction peaks attributable to Ni or Ni compounds were observed, but the formation of $Li_4P_2S_6$ was confirmed. After the 1st charge, the intensity of the diffraction peaks of $NiPS_3$ increased, indicating that $NiPS_3$ partially but reversibly reacted with Li^+ [Fig. 4(c)]. Nonetheless, we cannot deny the possibility that unreacted $NiPS_3$ was present. In addition, $Li_4P_2S_6$ was also detected after the 1st charge, suggesting that $Li_4P_2S_6$ was formed by an irreversible reaction [Fig. 4(c)].

Figures 5(a)–5(d) show the Ni K-edge XANES spectra of the as-prepared $NiPS_3$ and of the working electrodes after the 1st discharge, 1st charge, and 10th charge, respectively. After the first discharge, the absorption edge slightly shifted toward the low energy region, suggesting that the valence of nickel slightly decreased during the discharge process.[32] A weak absorption edge around 8330 eV was observed, similar to the absorption edge of Ni metal though the absorbance was much weaker [Fig. 5(e)]. The spectrum after the 1st charge [Fig. 5(c)] was different from that of the as-prepared sample but similar to that of the 10th charge [Fig. 5(d)].

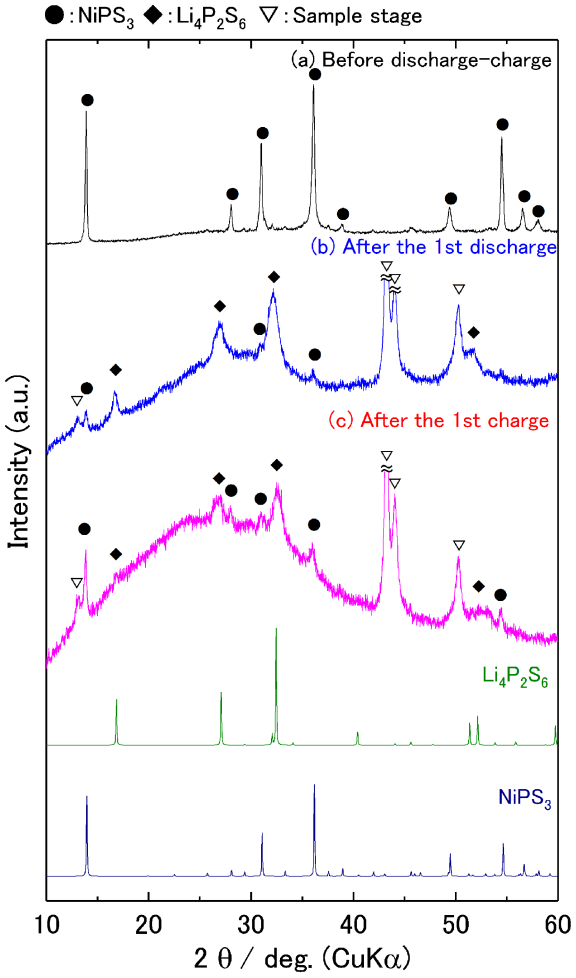

Fig. 4. XRD patterns of (a) as-prepared $NiPS_3$, and the working electrodes (b) after the 1st discharge and (c) after the 1st charge. The simulated diffraction patterns of $Li_4P_2S_6$ (ICSD #33506) and $NiPS_3$ (ICSD #646133) were also shown as references.

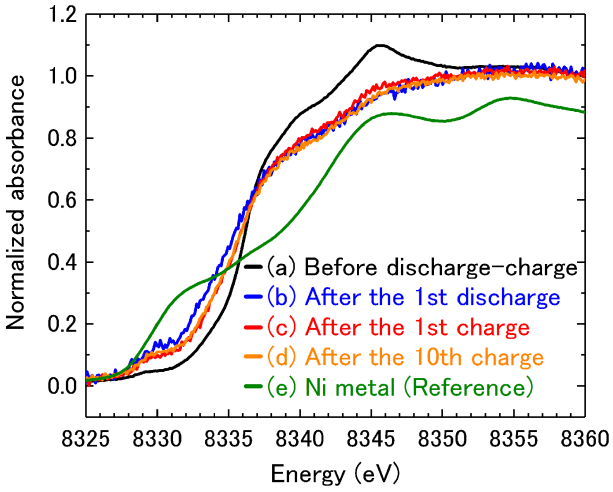

Fig. 5. Ni K-edge XANES spectra of (a) as-prepared $NiPS_3$, and the working electrodes (b) after the 1st discharge, (c) after the 1st charge and (d) after the 10th charge. (e) The spectrum of Ni metal is also shown as a reference.

4. Discussion

As shown in Fig. 4(c), diffraction peaks attributable to $NiPS_3$ were observed in the XRD pattern after the 1st discharge and charge. This result implies that $NiPS_3$ reversibly reacted (at least partially) with Li^+; however, there is a possibility that unreacted $NiPS_3$ remained after the 1st discharge and charge. The XANES spectra [Figs. 5(a) to 5(c)] clarified that the valence state of Ni slightly changed upon Li^+ insertion/extraction, but the change in the absorption edge was too small to explain the contribution of only Ni to charge compensation during discharge/charge. Thus, the redox reactions of S, as reported in TiS_3 and α-MoS_3,[33] could be responsible for this small change. In addition, an irreversible reaction would simultaneously occur during the 1st discharge process. In the XRD pattern after the 1st discharge [Fig. 4(b)], diffraction peaks indexed as $Li_4P_2S_6$ were detected and remained after the 1st charge [Fig. 4(c)]. Therefore, the formation of $Li_4P_2S_6$ can be formulated as follows:

$$2NiPS_3 + 4Li^+ + 4e^- \rightarrow Li_4P_2S_6 + 2Ni \qquad (2)$$

This irreversible reaction would reduce the initial capacity (Fig. 2). On the other hand, $Li_4P_2S_6$ is a moderate Li-conducting phase (2.38×10^{-7} S cm^{-1}).[34] Ni metal was not detected by XRD, but a weak X-ray absorption edge similar to that of Ni metal was detected, which can be explained by the formation of Ni nanoparticles smaller than ~2 nm or of low-crystalline phase(s) with low-valence Ni.

5. Conclusions

Submicron-sized $NiPS_3$ particles were successfully synthesized from fine Ni powder (<100 nm), red phosphorus, and sulfur by heat treatment at 673 K for 48 h. An all-solid-state lithium battery using the submicron-sized $NiPS_3$ as active cathode material showed a 10th discharge capacity of 147 mAh g^{-1} at 0.064 mA cm^{-2}, which is larger than that of a cell using 10–100 micron-sized $NiPS_3$. The reaction between $NiPS_3$ and Li^+ was barely accompanied by Ni redox, implying the redox reaction of S. In the 1st discharge (Li^+ insertion), an irreversible reaction producing $Li_4P_2S_6$ was observed. The irreversible formation of $Li_4P_2S_6$ should decrease the capacity but should not significantly hinder the conduction of Li^+ because of its moderate Li^+ conductivity.

Acknowledgements This work was supported by the Japan Science and Technology Agency (JST), Advanced Low Carbon Technology Research and development Program (ALCA), and Specially Promoted Research for Innovative Next Generation Batteries (SPRING) project.

Reference

1) M. Tatsumisago, M. Nagao and A. Hayashi, *J. Asian Ceram. Soc.*, 1, 17–25 (2013).
2) K. Takada, *Acta. Mater.*, 61, 759–770 (2013).
3) N. H. H. Phuc, K. Morikawa, T. Mitsuhiro, H. Muto and A. Matsuda, *Ionics*, 23, 2061–2067 (2017).
4) S. Yubuchi, S. Teragawa, K. Aso, K. Tadanaga, A. Hayashi and M. Tatsumisago, *J. Power Sources*, 293, 941–945 (2015).
5) R. C. Xu, X. L. Wang, S. Z. Zhang, Y. Xia, X. H. Xia, J. B. Wu and J. P. Tu, *J. Power Sources*, 374, 107–112 (2018).
6) A. Hayashi, S. Hama, H. Morimoto, M. Tatsumisago and T. Minami, *J. Am. Ceram. Soc.*, 84, 477–479 (2001).
7) H. J. Deiseroth, S. T. Kong, H. Eckert, J. Vannahme, C. Reiner, T. Zaib and M. Schlosser, *Angew. Chem. Int. Edit.*, 47, 755–758 (2008).
8) Y. Seino, T. Ota, K. Takada, A. Hayashi and M. Tatsumisago, *Energy Environ. Sci.*, 7, 627–631 (2014).
9) S. Ito, M. Nakakita, Y. Aihara, T. Uehara and N. Machida, *J. Power Sources*, 271, 342–345 (2014).
10) M. Calpa, N. C. Rosero-Navarro, A. Miura and K. Tadanaga, *RSC Adv.*, 7, 46499–46504 (2017).
11) M. Calpa, N. C. Rosero-Navarro, A. Miura and K. Tadanaga, *Inorg. Chem. Front.*, 5, 501–508 (2018).
12) N. Kamaya, K. Homma, Y. Yamakawa, M. Hirayama, R. Kanno, M. Yonemura, T. Kamiyama, Y. Kato, S. Hama, K. Kawamoto and A. Mitsui, *Nat. Mater.*, 10, 682–686 (2011).
13) Y. Kato, S. Hori, T. Saito, K. Suzuki, M. Hirayama, A. Mitsui, M. Yonemura, H. Iba and R. Kanno, *Nat. Energy*, 1, 16030 (2016).
14) F. Mizuno, S. Hama, A. Hayashi, K. Tadanaga, T. Minami and M. Tatsumisago, *Chem. Lett.*, 31, 1244–1245 (2002).
15) T. Matsuyama, A. Hayashi, T. Ozaki, S. Mori and M. Tatsumisago, *J. Mater. Chem. A*, 3, 14142–14147 (2015).
16) A. Sakuda, A. Hayashi and M. Tatsumisago, *Sci. Rep.*, 3, 2261 (2013).
17) S. Azuma, K. Aiyama, G. Kawamura, H. Muto, T. Mizushima, T. Uchikoshi and A. Matsuda, *J. Ceram. Soc. Jpn.*, 125, 287–292 (2017).
18) J. Haruyama, K. Sodeyama, L. Han, K. Takada and Y. Tateyama, *Chem. Mater.*, 26, 4248–4255 (2014).
19) K. Takada, N. Ohta and Y. Tateyama, *J. Inorg. Organomet. P.*, 25, 205–213 (2015).
20) B. Wu, S. Wang, W. J. Evans, IV, D. Z. Deng, J. Yang and J. Xiao, *J. Mater. Chem. A*, 4, 15266–15280 (2016).
21) A. Sakuda, H. Kitaura, A. Hayashi, K. Tadanaga and M. Tatsumisago, *J. Electrochem. Soc.*, 156, A27–A32 (2009).
22) A. Sakuda, A. Hayashi and M. Tatsumisago, *Chem. Mater.*, 22, 949–956 (2010).
23) N. Ohta, K. Takada, I. Sakaguchi, L. Zhang, R. Ma, K. Fukuda, M. Osada and T. Sasaki, *Electrochem. Commun.*, 9, 1486–1490 (2007).
24) H. Kitaura, A. Hayashi, K. Tadanaga and M. Tatsumisago, *Electrochim. Acta*, 55, 8821–8828 (2010).
25) K. Ohara, A. Mitsui, M. Mori, Y. Onodera, S. Shiotani, Y. Koyama, Y. Orikasa, M. Murakami, K. Shimoda, K. Mori, T. Fukunaga, H. Arai, Y. Uchimoto and Z. Ogumi, *Sci. Rep.*, 6, 21302 (2016).
26) R. Brec, *Solid State Ionics*, 22, 3–30 (1986).
27) Y. V. Kuzminskii, B. M. Voronin and N. N. Redin, *J. Power Sources*, 55, 133–141 (1995).
28) Y. V. Kuzminskii, B. M. Voronin, I. M. Petrushina,

N. N. Redin and G. P. Prikhodko, *J. Power Sources*, 55, 1–6 (1995).
29) Y. Fujii, Y. Suto, A. Miura, M. Higuchi and K. Tadanaga, *Chem. Lett.*, 45, 652–654 (2016).
30) Y. Fujii, A. Miura, N. C. Rosero-Navarro, M. Higuchi and K. Tadanaga, *Electrochim. Acta*, 241, 370–374 (2017).
31) E. Prouzet, G. Ouvrard and R. Brec, *J. Power Sources*, 26, 319–324 (1989).
32) T. Takeuchi, H. Sakaebe, H. Kageyama, T. Sakai and K. Tatsumi, *J. Electrochem. Soc.*, 155, A679–A684 (2008).
33) T. Matsuyama, M. Deguchi, K. Mitsuhara, T. Ohta, T. Mori, Y. Orikasa, Y. Uchimoto, Y. Kowada, A. Hayashi and M. Tatsumisago, *J. Power Sources*, 313, 104–111 (2016).
34) Z. D. Hood, C. Kates, M. Kirkham, S. Adhikari, C. Liang and N. A. W. Holzwarth, *Solid State Ionics*, 284, 61–70 (2016).